Automation in Construction 159 (2024) 105289

Contents lists available at ScienceDirect

Automation in Construction

journal homepage: www.elsevier.com/locate/autcon

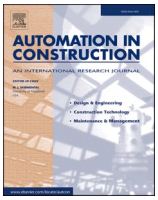

Development of nomograms for the prediction of inherent geometric defects in stone block pavements

Erika Garilli *, Nazarena Bruno, Federico Autelitano, Felice Giuliani

Dipartimento di Ingegneria e Architettura, Università di Parma, Parco Area delle Scienze 181/A, Parma 43124, Italy

ARTICLE INFO

Keywords:
Stone pavement
Surface drainage
Inherent defects
Joints
Vertical misalignments
3D virtual analysis

ABSTRACT

Stone block pavements consist of discrete units placed closed together and embedded in a bound or unbound bedding layer according to a given laying pattern. Such pavements are widespread in historic and architecturally valuable urban centres. Design choices, including laying pattern, cross-sectional shape, and slope, are not exempt from causing inherent defects such as joint openings and height differences between adjacent elements, depending on the sizes of the individual stone blocks. Prior knowledge of the deviation of the actual surface from the ideal one allows such problems to be managed during the design, execution and validation phases of the work and is essential for resolving disputes between the client and the contractor. Following the analysis of a 3D virtual reconstruction of stone block pavements, the authors developed nomograms for the quantitative prediction of inherent geometric defects in relation to the parameters influencing their values.

1. Introduction

Stone block pavements (SBPs) belong to the elemental or segmental pavement (SP) broader family, in which the surface course consists of discrete units placed close together and embedded in a bound or unbound bedding layer (Fig. 1) [1–3]. The dimensional characteristics of natural stone elements, as well as their surface finishing (of both the side and top faces), are important morphological variables. Unlike industrial products, which are strictly controlled in tolerances and modularity, slight deviations of stone paving elements from the standard dimensions are tolerable [1,4,5]. Due to these variabilities, resulting from quarrying, cutting and dressing process, the pavement surface may show irregularities, which affect the aesthetic performance, the mechanical behaviour of the pavement, the water disposal, the joint network and the interaction of different users with the pavement itself (skid resistance and slip potential) [6,7]. These irregularities can be defined supply defects. As for the joints, which are the gaps or distances between paving blocks, they represent especially important parts of the paving system performing numerous tasks, such as stabilize blocks, transmit loads to the adjacent blocks and dissipate them in the underlying courses, control the water drainage, etc. [6,8]. Once more, dimensional variabilities of stone elements affect the joint geometry, leading to surface irregularities that compromise the aesthetic result and the mechanical resistance of the paving, as well as reduce the users' safety and comfort: these irregularities are again defined supply defects. The tolerance of these defects varies according to the users [7,9,10]. Since SBPs can be adopted in pedestrian and cycling facilities, in areas receiving no commercial vehicular traffic or in roads used by a low to medium number of city heavy vehicles, the choice of dimensional characteristics of the stone elements and joints, as well as the selection of the pavement structure type (flexible, semi-rigid or rigid), depend on the site category [11]. Laying defects, which are those in which surface irregularities are due to improper pavement construction attributable to the pavers, can also be identified in addition to supply defects. However, there are situations where surface irregularities are attributable neither to supply defects nor to laying defects, but to inherent characteristics of SBPs.

The construction of continuous pavements, in which asphalt or concrete courses are laid using vibratory pavers and the surface finishing is done by roller-compactors and screed vibrators respectively, produce homogeneous and regular surfaces capable of following the longitudinal and transverse design profile. On the other hand, individual elements are placed by hand and compacted using a vibrating plate or a hand tamper in the construction of SBPs. Contrary to asphalt and concrete mixtures, such blocks are rigid elements which may not be able to adequately match the transverse and longitudinal design profile due to their shapes, sizes, and laying patterns. In general, the choice of the cross-sectional profile of a road surface depends on several factors such as the traffic type, the road width, its plano-altimetric profile, the type of

* Corresponding author.
E-mail address: erika.garilli@unipr.it (E. Garilli).

https://doi.org/10.1016/j.autcon.2024.105289
Received 8 May 2023; Received in revised form 15 January 2024; Accepted 16 January 2024
0926-5805/© 2024 The Authors. Published by Elsevier B.V. This is an open access article under the CC BY-NC-ND license (http://creativecommons.org/licenses/by-nc-nd/4.0/).

pavement surface and of water drainage, etc. [5,12]. Excluding dynamic effects, which are not relevant in urban areas, an ideal road surface should be perfectly flat, and the only purpose of introducing camber is to quickly drain rainwater falling on the roadway [13–15]. The shape of the road section can be represented by an upward or downward concave line [1,16]. The upward concave section, with central water drainage, can still be found in alleys of some historical urban centres; but in almost all cases an upward convex section, with lateral water drainage involving less vehicular interference, is adopted. The shape most widely used to date, mainly due to the simplicity of construction, is the straight camber, which is provided by meeting two straight surfaces in the crown. However, it is not optimal for water drainage and presents problems in case of distress [17]. Multi-slope camber was chosen to overcome this issue. It consists of two or three straight lines that are steeper near the edges and relatively flatter near the crown portion of the pavement [18]. Then, there are more complex non-linear sections developed in the past to optimize the water runoff on different kinds of pavements. These include the circular camber in which the shape of road section is represented by a circular arc [15,17]. The arc radius depends on the roadway width, while the camber is more or less pronounced to improve the water runoff: a road with non-zero longitudinal slope requires a smaller curvature [19,20]. However, this configuration has an excessive slope at the sides for wide roadways (>4 m). Thus, other profiles, such as the composite and the parabolic cambers, were adopted to overcome this issue. These considerations are critically important in the choice of such architectural-value profiles, when the pavement is located in a nineteenth-century-type layout and needs to be specifically joined with sidewalks and/or accesses of historically designed buildings. The composite profile consists of a circular crown at the centre of the camber and two straight slopes originating from the edges, which allows the slope to be reduced in the side strips of the roadway [15–17,19,20]. As far as the cross section of parabolic shape is concerning, a cubic parabola for non-erodible pavements [17] or a second-order parabola for other pavements [19,21] have been the most used profiles in the past: the roadway surface is flatter in the crown area by quicker sloping to the edges [14,15].

As previously mentioned, stone blocks are rigid elements having specific geometric characteristics and they may not be able to match the transverse and longitudinal design profile. Such peculiarities can cause several drawbacks regarding the pavement structure and issues for the road users' comfort and safety, as a function of the site categories [7,22]. The variation in the width of the joints (compared to the design joint width), can compromise the aesthetic result and the mechanical resistance of the paving, as well as reduce the users' comfort. The height differences between adjacent elements can lead to both comfort and safety issues in pedestrian-only areas, especially in presence of impaired users, cycling facilities and areas subject to vehicular traffic; this defect can also lead to the initiation of further damage during winter maintenance operations (interaction with snowplow blades). The variation of the joint width and the height differences between adjacent elements can be seen as inherent SBPs' defects. In this study only the inherent SBPs' defects were quantitatively analysed by the 3D virtual reconstruction, accounting for different cross section profiles, laying patterns and stone block dimensions. The analyses provided the evaluation of opening or closing of joints and height differences between adjacent elements and the identification of the most critical areas. Then, useful nomograms were implemented to simulate and prefigure unevenness between adjacent elements according to the laying characteristics: these graphs can be adopted in the design and validation of SBPs as well as in the case of disputes between client and contractor.

2. Issues related to cross-section shape of SBPs

Stone road pavements may have cross sectional profiles with different shapes (linear or curvilinear) and slopes depending on several factors, such as traffic categories, water drainage, road width, type of used elements (shape, size, material, surface finish etc.), laying pattern and weather conditions. Stone blocks and flagstones are rigid elements with a rectangular cuboid shape (i.e., their faces are rectangular and parallel two by two): the first ones are deep elements (>100 mm thick) typically used in streets and roads, while the second ones are shallow units (50 to 100 mm thick) typically used in pedestrian areas (footpaths, squares, arcades) with occasional vehicular traffic [5]. The use of these kind of stone elements can generate defects that are insurmountable from a design and construction point of view. The main defects are represented by the variation in the joint width (compared to the design joint width) and the possible generation of vertical misalignments between adjacent elements. Such defects, in turn, depend on numerous factors such as the dimensions (width, length and thickness) of the individual elements, their shape (of both top and side faces), their layout in the horizontal plane, the width of the pavement, the shape of its cross-section, its slope, etc.. Limiting the joint width and unevenness between

Fig. 1. Construction of a street pavement using igneous stone blocks.

adjacent blocks during design and construction phases, and checking it during the validation phase, are necessary practices to avert these eventualities.

2.1. Excessive or low joints width

Stone blocks or flagstones must be placed close together to each other on the bedding layer, to obtain a distance between adjacent elements equal to design joint width (j_d), following the longitudinal and transversal profile of the road surface. As can be seen in Fig. 2, due to the shape of the elements and the non-straight cross section, the joints cannot maintain a constant width through the entire thickness of the surface course. For this reason, the actual joint width will be different from the design one. However, joints represent an especially important part of the paving system performing numerous [6,22]; too wide or irregular joints can compromise the aesthetic result and the mechanical resistance of the paving, as well as reduce the users' comfort.

2.2. Unevenness between adjacent elements

In addition to a non-constant joint width, the rectangular cuboid-shaped elements and the non-straight cross section shape may produce, for some laying patterns, height differences between adjacent elements (*hd*): an example is shown in Fig. 2. These differences can result in comfort but also safety issues for different types of users (pedestrians, cyclists, drivers, etc.).

3. Experimental structure

3.1. Definition of analysed cross sections

Four cross sections were analysed in this study, i.e., the straight, the multi-slope, the Allard parabolic (second-order parabola) and the cubic parabolic cambers (Fig. 3). The straight camber is the most widely used cross-section. It consists of two straight surfaces, meeting in the crown, which have a transverse slope s_t. In addition, the crown has an elevation c, hence $s_t = \frac{2c}{W}$ where W is the roadway width. Taking an edge of the road as a reference, the camber coordinates can be calculated from Eq. (1):

$$\begin{cases} y = 2cx = s_t x & 0 \le x < \dfrac{W}{2} \\ y = s_t(W - x) & \dfrac{W}{2} \le x \le W \end{cases} \tag{1}$$

Since the other cambers have variable slopes across the cross-section, an equivalent slope $s_e = s_t$ was considered. The selected multi-slope camber is a three-straight line camber. Starting from the roadway edges, the first section (length of about $W/8$) has a slope $s_1 = 1.5s_e$, the second section (length of $W/4$) has a slope $s_2 = s_e$ and the third section, close to the centreline, has a slope $s_3 = s_e/2$. The camber coordinates can be calculated from Eq. (2):

$$\begin{cases} y = 1.5s_e x & 0 \le x < \dfrac{W}{8} \\ y = 1.5s_e\dfrac{W}{8} + s_e\left(x - \dfrac{W}{8}\right) & \dfrac{W}{8} \le x < \dfrac{3W}{8} \\ y = 1.5s_e\dfrac{W}{8} + s_e\dfrac{W}{4} + \dfrac{s_e}{2}\left(x - \dfrac{3W}{8}\right) & \dfrac{3W}{8} \le x < \dfrac{W}{2} \\ y = 1.5s_e\dfrac{W}{8} + s_e\dfrac{W}{4} + \dfrac{s_e}{2}\left(\dfrac{5W}{8} - x\right) & \dfrac{W}{2} \le x < \dfrac{5W}{8} \\ y = 1.5s_e\dfrac{W}{8} + s_e\left(\dfrac{7W}{8} - x\right) & \dfrac{5W}{8} \le x < \dfrac{7W}{8} \\ y = 1.5s_e(W - x) & \dfrac{7W}{8} \le x \le W \end{cases} \tag{2}$$

Allard's parable was chosen as the second-order parable [12]. The camber coordinates can be calculated from Eq. (3):

$$y = c - \frac{d}{W - \frac{W}{8}}\left(x - \frac{W}{2}\right)^2 \tag{3}$$

in which $d = 4k$ is the vertical gap between the defense point and the water line (Fig. 4) and the k parameter can be calculated starting from Eq. (4):

$$c = k\frac{W^2}{W - \frac{W}{8}} \tag{4}$$

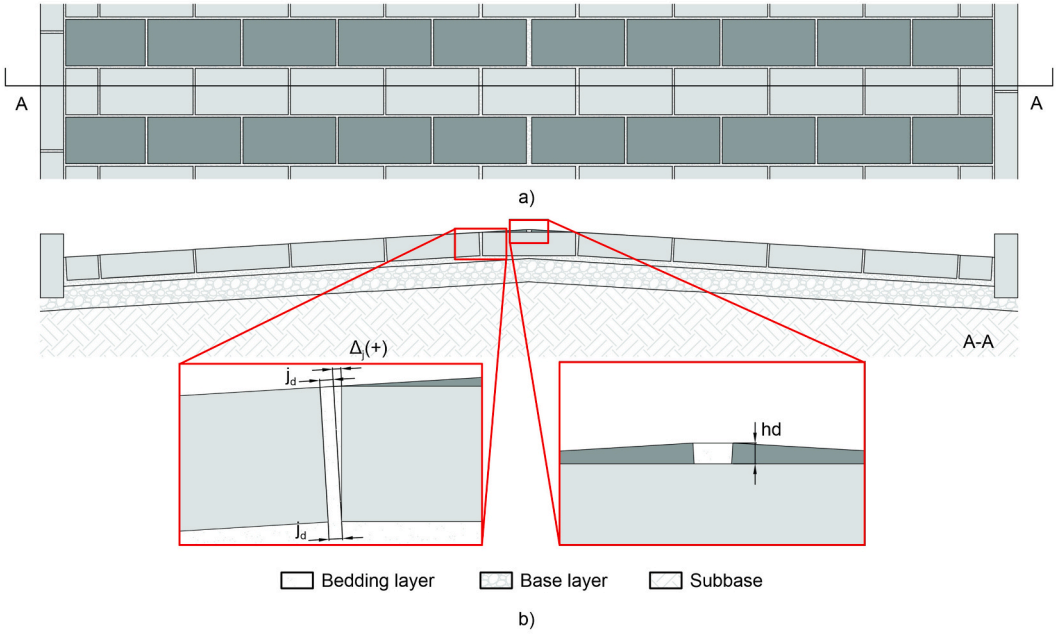

Fig. 2. Pavement with straight camber and stretcher bond laying pattern: a) plan view and b) section with emphasis on joint openings and height differences between adjacent elements.

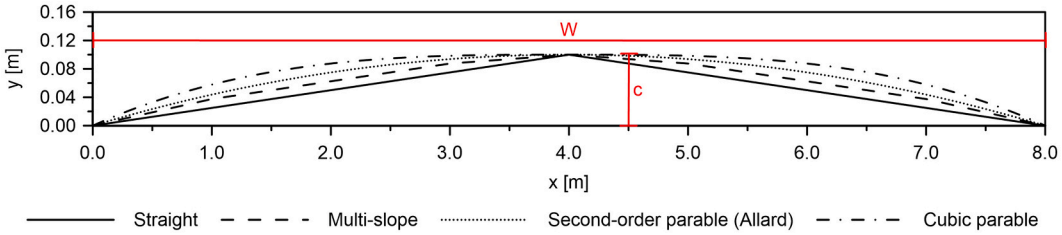

Fig. 3. Analysed cross-section shapes.

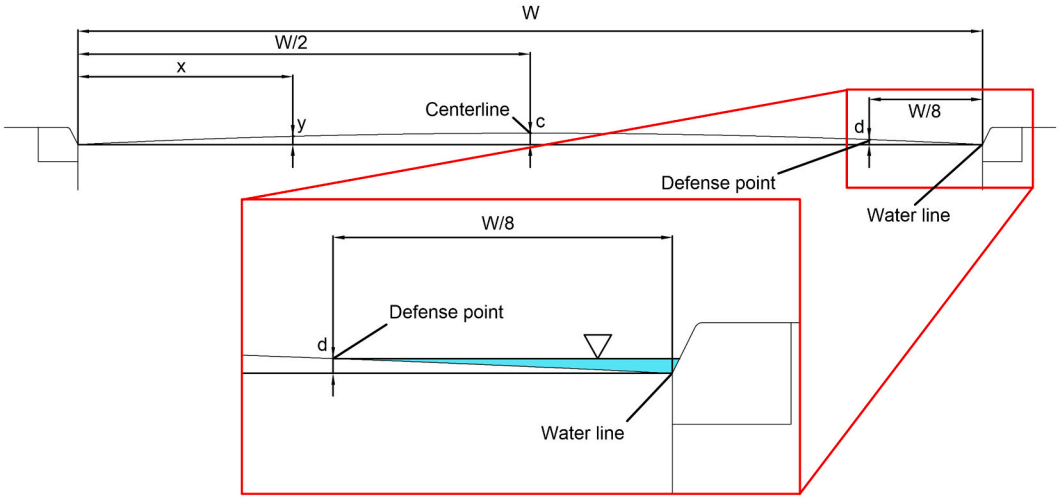

Fig. 4. Allard's second-order parable camber.

Finally, the cubic parabolic camber coordinates can be calculated from Eq. (5):

$$\begin{cases} y = \dfrac{W}{2}s_e + \dfrac{s_e}{\left(\frac{W}{2}\right)^2}\left(x - \dfrac{W}{2}\right)^3 & 0 \le x < \dfrac{W}{2} \\ y = \dfrac{W}{2}s_e - \dfrac{s_e}{\left(\frac{W}{2}\right)^2}\left(x - \dfrac{W}{2}\right)^3 & \dfrac{W}{2} \le x \le W \end{cases} \quad (5)$$

3.2. Definition of analysed laying pattern

Five laying patterns were analysed: the stacked bond or running bond in which the stone blocks are aligned in both transversal and longitudinal directions (Fig. 5a), the stretcher bond in which the stone blocks are aligned in transversal direction but staggered in the longitudinal one (Fig. 5b), the herringbone tilted by 45° consisting of parallel stone blocks slanting in alternate directions to form a series of parallel Vs or zigzags (Fig. 5c), the stretcher bond tilted by 45° (Fig. 5d) and the converging stretcher bond similar to the stretcher bond tilted by 45° but with the centreline acting as symmetry axis (Fig. 5e).

A reference pavement made of 80 cm long, 40 cm wide and 20 cm

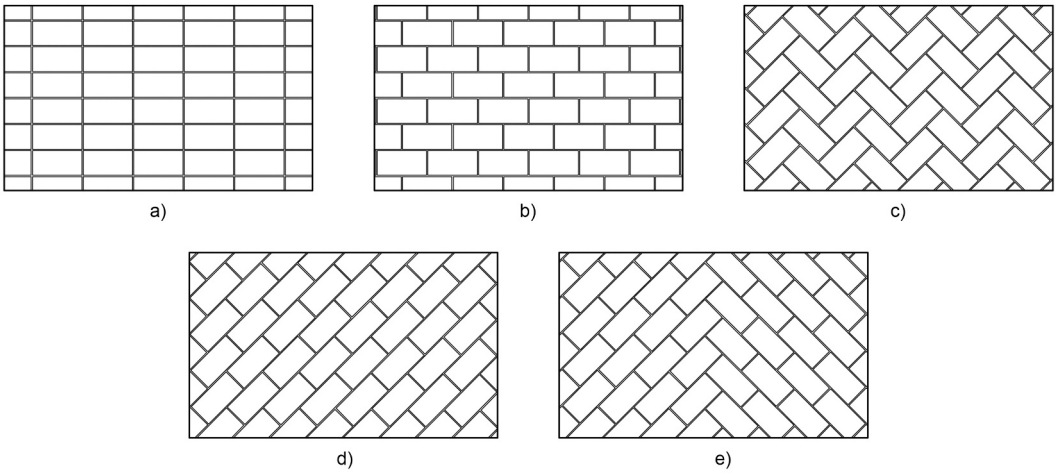

Fig. 5. Analysed laying patterns: a) stacked bond or running bond, b) stretcher bond, c) herringbone tilted by 45°, d) stretcher bond tilted by 45° and e) converging stretcher bond.

thick stone blocks was analysed in this study: these large elements accentuate all the installation problems described in section 3. A roadway width of 8 m was then chosen for the reference analysis so that it could be compared to an existing urban roadway. The crown was chosen equal to 1/80th of the roadway width ($c = W/80 = 10\ cm$) to have an equivalent slope of 2.5%, which is typically used for urban roads.

4. Analysis methods

A 3D virtual reconstruction of the analysed SBPs was created to figure out the joints opening or closing, as well as the height difference between adjacent elements. The simulation allowed to study the vertical misalignments between adjacent elements in a controlled working environment and to test different configurations quickly and without the need to make a physical model. Moreover, assessment metrics can be quickly and dynamically extracted from the 3D model by creating sections or profiles and by making comparisons with ideal laying configurations, without the need to survey the physical model. The 3D model was created using the AutoCAD software [23]. Two sets of 3D elements were generated: the first one is the bedding layers considering the different cross-sectional cambers, while the second one is the stone blocks arranged according to the different laying patterns. The 3D blocks have been placed on the bedding layer surface through a series of roto-translations of the individual elements. Since stone blocks are rigid elements and the bedding layer has cross-sectional camber, the laying of the blocks cannot perfectly adhere to the camber profile, but it represents its discretization. In physical laying operations, the bedding layer is adjusted by adding or removing material as needed. In the simulation, the different stiffness of stone blocks and bedding layer were considered, and the block were laid with the extremities tangent to the curvature, while the middle part was assumed to be secant to the bedding layer, thus considering an ideal material removal. This resulted in a laying surface divergent from the theoretical one and in joint sizes variations, which depend on the position of the block along the cross-sectional camber and on the laying pattern, as occurs in the real laying operations. These defects of the laying have been analysed and presented in sections 4.1 and 4.2.

4.1. Opening or closing of the joint

The joint network is one of the most important parts of the stone paving system, performing multiple tasks. Joints are characterized by their width, jointing material, degree of filling, which influence the overall behaviour of the pavement [12,24–26]. Joints may present a loss of filling material decreasing the strength of the whole pavement, leading to its rapid deterioration, due to poor maintenance of the joints and/or incorrect design and execution of them (too wide or too narrow, not fully saturated, wrong choice of material, etc.) [10,27]. For this reasons, it is necessary that the joints are properly made and that their characteristics are checked during acceptance testing [5]. The measurements of the joints' width were made on the AutoCAD 3D model, as illustrated in Fig. 2, to analyse the SBPs joints opening or closing. Vertical cross-section planes were drawn by cutting the different models at key points, corresponding to the vertices of the blocks' upper faces. In extracting the data, a curb with a lateral surface parallel to the lateral surface of the first block constituting the analysed pavement was assumed for both lateral edges of the roadway. The width of a joint at the bottom (in contact with the bedding layer) was taken as a reference and equal to the design joint width (j_d). The difference (Δj) between the top joint width (j_t) and the bottom one (j_d) is equal to the joint opening ($\Delta j > 0$) or closing ($\Delta j < 0$). The percentage change in the joint width was considered to better compare the different analysed solutions (Eq. (6))

$$\Delta j[\%] = \frac{j_t - j_d}{j_d} \times 100 \tag{6}$$

4.2. Unevenness between adjacent elements

For the evaluation of the height difference between adjacent elements on the pavement top surface, a first analysis was carried out by comparing the top surfaces resulted after laying the blocks and the theoretical smooth surface corresponding to the camber of the investigated cross-section. The mesh obtained from each different configuration was compared with the mesh surface model of the just mentioned theoretical shape, assumed as reference. All the different combinations were evaluated. The analysis was performed with the CloudCompare software [28], which is an open-source 3D point cloud and triangular mesh processing software. The software computes the distances between the vertices of the compared mesh (the pavement top surface) and the nearest polygon face of the reference mesh. The results can be shown also using a scalar field and, from the false-colour obtained images, the critical points for the different laying patterns and cross-section curvature were identified. Using AutoCAD, longitudinal sections passing through these points were then extrapolated, along which height differences were measured.

5. Results and discussions

5.1. Opening or closing of the joint for reference parameters

For each laying pattern, four cross sections passing through the key points corresponding to the vertices of the top faces of the blocks were identified and analysed, except for the stacked bond laying pattern where the regularity of the blocks' laying makes only two sections significant. Fig. 6 shows the results of each remarkable section and laying pattern.

As far as the stacked bond laying pattern is concerned (Fig. 6a), the two sections A-A and B-B provide the same results for all the selected cross-sectional profiles. In the case of the straight camber, the joint on the roadway centreline is open, while all other joints are unchanged. For the Allard camber, a constant Δj [mm] is observed: for the selected roadway width, the second-order parabola camber is almost coincident with a circular camber in which the increase in slope from the centreline toward the edges is constant. For the cubic profile, moving from the sides toward the centreline Δj [mm] decreases: the change in slope decreases moving from the edges toward the centreline. Finally, for the multi-slope camber, in which the change in slope does not occur continuously, the three centre joints do not respect the previously described decreasing trend: the reason is that there is a cusp in the centreline and the two points straddling it are at a distance of about 80 cm from the centreline (length of the slab) and the next slabs will have the change in slope below it.

In the stretcher bond laying pattern (Fig. 6b) the pairwise cross section (A-A with B-B and C-C with D-D) provide the same Δj[mm] values. In the case of the straight profile, the joints on the roadway centerline (the one directly on the centerline for the cross sections A-A and B-B and those close to the slab abutting the centreline for cross section C-C and D-D) are open: like the stacked bond laying pattern, all other joints are unchanged. For the Allard camber, a constant Δj[mm] value occurs except for the joint near to the centreline for section C-C and D-D where there is a decrease in Δj[mm]. Multi-slope and cubic parable camber follow the same trend highlighted in the stacked bond laying pattern.

In the case of herringbone 45° (Fig. 6c), stretcher bond 45° (Fig. 6d) and converging stretcher bond laying patterns (Fig. 6e) the four identified cross sections show different trends from each other. In the herringbone 45° laying pattern a large part of the joints tends to slightly close. The critical points are straddling the centreline for the straight and

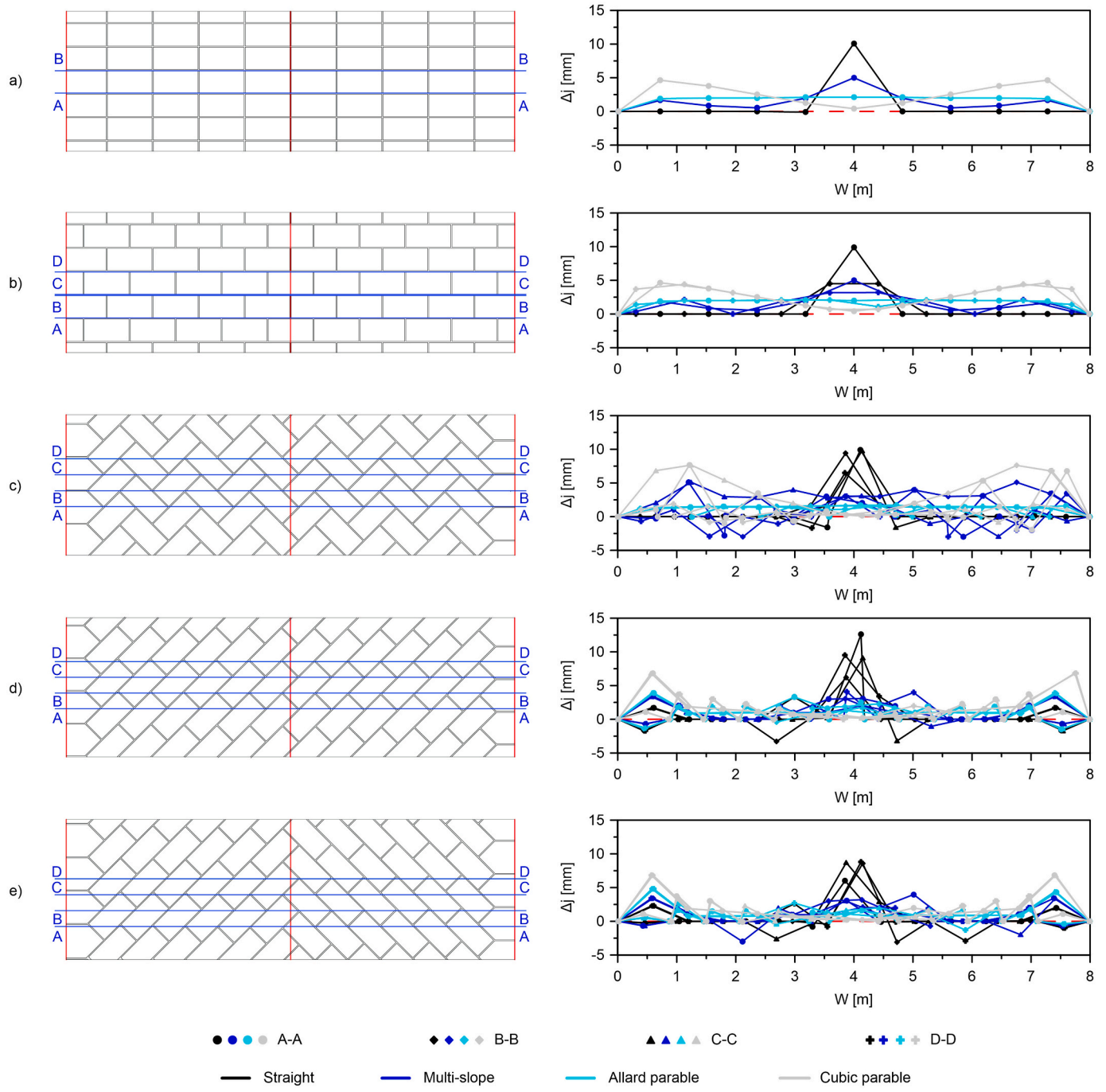

Fig. 6. Δj [mm] trend for different cross-section shape: a) stacked bond laying pattern; b) stretcher bond laying pattern; c) herringbone tilted by 45° laying pattern; d) stretcher bond tilted by 45° laying pattern; e) converging stretcher bond laying pattern.

the multi-slope camber, while for the second order and cubic parabolic camber such variations are the same over the entire cross-section.

5.2. Opening or closing of the joints as a function of different parameters

During an acceptance test, or an on-site verification of the successful laying of stone elements, it is possible to measure the upper joint width. But, an analytical formulation is necessary to determine the maximum joint opening as a function of some geometric parameters to have a theoretical comparative value as a preventive measure. Thus, the stretcher bond laying pattern was taken as a reference to evaluate the influence of the block thickness (t) and length (L), the crown (and consequently the equivalent slope s_e), the joint design width (j_d) and the roadway width (W) on the joints' opening. In this specific case, the width of the stone blocks is not included in the parameters affecting the width of the joints since it is in the direction perpendicular to the cross section. For each cross section and for each pair of sections (A-A with B-B and C-C with D-D), the maximum percentage changes of the joints were determined, first as a function of stone block thickness ($\Delta j_{\%}(t)$), keeping fixed the equivalent slope, then as a function of equivalent slope ($\Delta j_{\%}(s_e)$), keeping fixed the thickness of the stone block. Some examples of the maximum $\Delta j_{\%}(t)$ and $\Delta j_{\%}(s_e)$ referred to the straight and the Allard parabolic cambers are shown in Fig. 7.

As can be seen, the points are well interpolated by straight lines passing through the origin for both cambers. For all cross-sectional analysed shapes, $\Delta j_{\%}$ increases as both t and s_e increase. The greatest

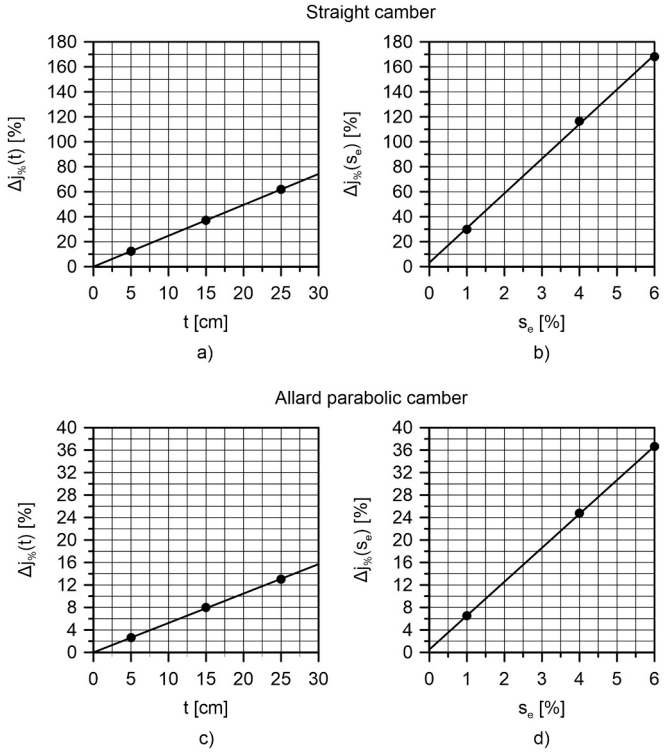

Fig. 7. Maximums a) $\Delta j_{\%}(t)$ (with $s_e = 2.5\%$) and b) $\Delta j_{\%}(s_e)$ (with $t = 30\ cm$) for straight camber and c) $\Delta j_{\%}(t)$ (with $s_e = 2.5\%$) and d) $\Delta j_{\%}(s_e)$ (with $t = 30\ cm$) for Allard parabolic camber.

growth, as a function of both t (with $s_e = const$) and s_e (with $t = const$), was observed for the straight camber with double growth compared to the multi-slope camber, 2.6 times compared to the cubic parabolic camber, and 4.7 compared to the Allard camber, which is thus the section with the lowest growth. For all the considered combinations, the maximum $\Delta j_{\%}$ was observed in the central part for the straight and the multi-slope cambers, in the lateral part for the cubic parabolic camber while it was constant along the whole section for the Allard camber. The fitting equations found in the two cases have the same form, and it is therefore possible to identify a function that considers both parameters.

The use of graphs that quantify the percentage of joint opening on the theoretical joint, as a function of cross section slope and slab thickness, can be highly effective for application purposes. An example of $\Delta j_{\%}(s_e, t)$ obtained for the Allard camber is represented in Fig. 8.

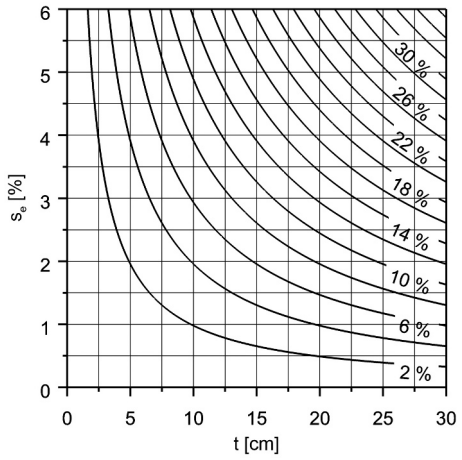

Fig. 8. $\Delta j_{\%}(s_e, t)$ for Allard camber and stretcher bond laying pattern.

The same analysis was conducted by varying the other parameters one at a time i.e., block length (L), joint design width (j_d) and roadway width (W). An example of the trends of $\Delta j_{\%}$ as a function of j_d ($\Delta j_{\%}(j_d)$) for the straight camber is shown in Fig. 9a. As can be seen, $\Delta j_{\%}(j_d)$, by fixing s_e and t, can be interpolated with a power function $\Delta j_{\%}(j_d) = \alpha \times j_d{}^{\beta}$, in which α and β depend on s_e and t.

In order to find the trend of $\Delta j_{\%}$ independently of the previously obtained values, i.e., $\Delta j_{\%}(t)$ and $\Delta j_{\%}(s_e)$, it was decided to calculate a coefficient c_n (with $n = 1$ for slab length, $n = 2$ for joint design width, and $n = 3$ for roadway width) obtained by Eq. (7)

$$c_n = \frac{\Delta j_{\%}(n_v)}{\Delta j_{\%}(n_{v\_ref})} \tag{7}$$

in which n_v is the parameter value (L, j_d or W), and n_{v_ref} is the parameter reference value (L=80 cm, j_d=20 mm and W=8 m). An example of $c_2(j_d)$ for the straight camber is shown in Fig. 9b: also the $c_2(j_d)$ can be interpolated by a power function.

By repeating these analyses for the different cross sections, the nomograms represented in Fig. 10 can be drawn. The maximum expected joint width at the surface (j_{max}) can be calculated through Eq. (8):

$$j_{max} = j_d \times \left(1 + \frac{\Delta j_{\%}(t, s_e)}{100} \times c_1 \times c_2 \times c_3\right) \tag{8}$$

in which j_d is the joint design width, $\Delta j_{\%}(t, s_e)$ can be read from the left nomograms and c_1, c_2 and c_3 from the right nomograms of Fig. 10.

A practical example of using nomograms to determine the maximum expected width of the joint is given. A pavement made with stone blocks having a length of 50 cm and a thickness of 15 cm arranged in a stretcher bond laying pattern is considered. The joint design width is set to 10 mm. The cross section has a cubic parabolic shape with an equivalent slope equal to 3%. The roadway width is 7 m. It is necessary to refer to the Fig. 10c to solve this problem. From the first nomogram it is possible to determine:

$$\Delta j_{\%}(t, s_e) = \Delta j_{\%}(15, 3) = 16\%$$

$$c_1(L) = c_1(50) = 0.74$$

$$c_2(j_d) = c_2(10) = 1.83$$

$$c_3(W) = c_3(7) = 1.13$$

At this point maximum joint width at the surface (j_{max}) can be calculated as:

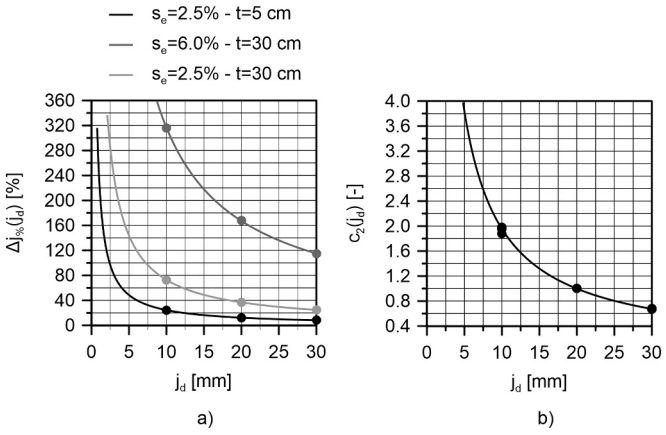

Fig. 9. a) $\Delta j_{\%}(j_d)$ vs j_d and b) $c_2(j_d)$ vs j_d for straight camber and stretcher bond laying pattern.

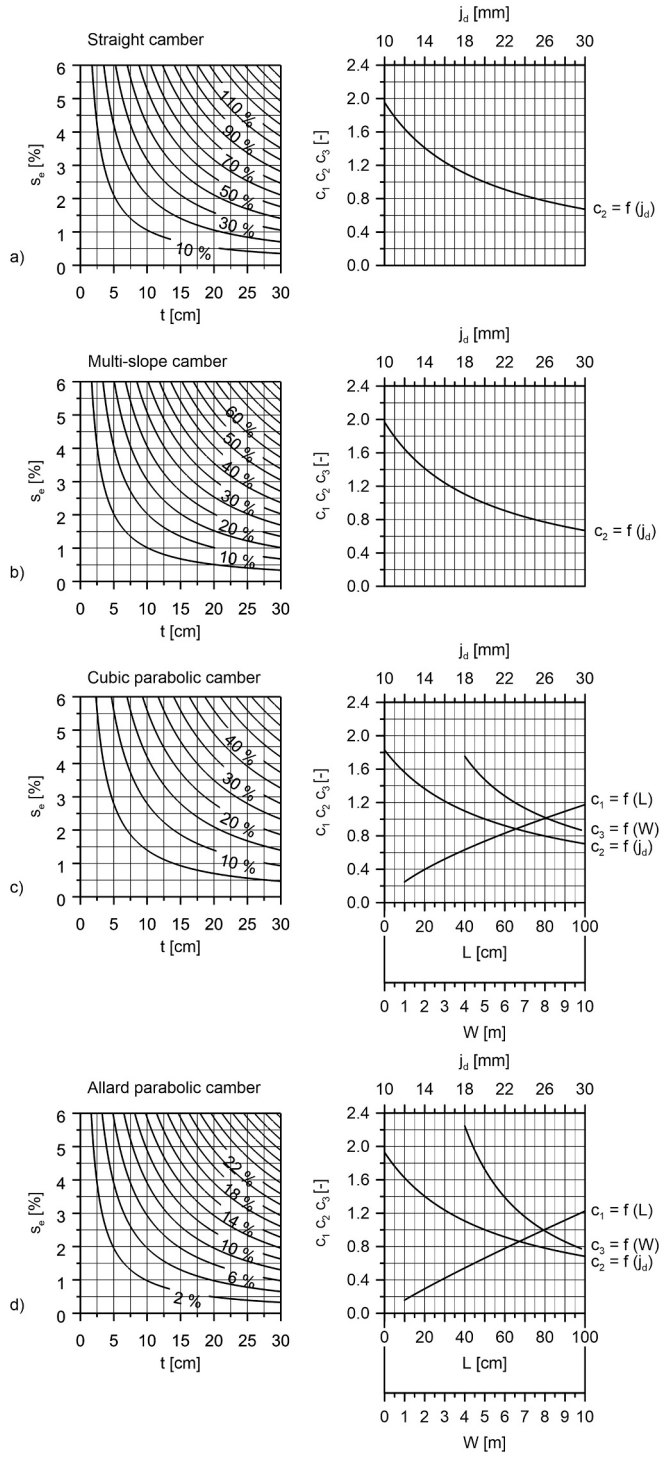

Fig. 10. Nomogram for determination of j_{max} for stretcher bond laying pattern and a) straight, b) multi-slope, c) cubic parabolic and d) second order (Allard) parabolic camber.

$$j_{max} = j_d \times \left(1 + \frac{\Delta j_{\%}(t, s_e)}{100} \times c_1 \times c_2 \times c_3\right)$$
$$= 10 \times \left(1 + \frac{16}{100} \times 0.74 \times 1.83 \times 1.13\right) = 12.4\ mm.$$

5.3. Unevenness between adjacent elements for reference parameters

For the evaluation of the height difference between adjacent elements on the pavement surface, a first analysis was conducted by analysing the different configurations with CloudCompare. Having set the longitudinal slope equal to 0% all the blocks should be at the same level but, as already mentioned, because stone blocks are rigid elements an adjustment of the bedding layer is required. In fact, in some parts, it will be necessary to increase the layer thickness by adding material while in other parts to remove material: this will generate a new surface that diverges from the theoretical one. Examples of the false-colour images obtained with CloudCompare are shown in Fig. 11. The colour scale indicates the level of the block pavement upper surface compared with the level of the theoretical upper surface of the bedding layer (without thickness adjustment of this layer). The critical longitudinal sections, i.e., those at which there is the maximum height difference (*hd*) between two adjacent elements, can be identified thanks to this representation. This analysis refers to the reference pavement, i.e., an 8 m wide roadway consisting of 80 cm long, 40 cm wide and 20 cm high blocks spaced 20 mm apart. A summary of the maximum height differences between adjacent elements and their localization according to different laying patterns and cross-section shapes is shown in Table 1.

The stacked bond laying pattern is the only one that always returns a null *hd* value: blocks belonging to adjacent rows show the same rotation. Despite from a user comfort point of view this laying pattern represents the ideal solution, it is well known that this configuration can lead to a rapid deterioration of the pavement due to the alignment of the joints, which are the most vulnerable items of the surface, in the direction of the traffic flow [6,29]: such alignments can lead to horizontal displacement mainly induced by the horizontal component of vehicular loads transmitted to the pavement under conditions of adherence during breaking, accelerating and turning manoeuvres.

5.4. Unevenness between adjacent elements as a function of different parameters

During the design phase of a stone road pavement, indistinctly intended for vehicular, bicycle or pedestrian traffic, it is necessary to meet not only the structural requirements but also the safety and comfort ones. Unevenness on the road surface can lead to a reduction in comfort, with vibration and noise generation (whether for car, motorcycle, or bicycle drivers, wheelchair users, pedestrians pulling or pushing an object such as a suitcase trolley, etc.), but also to a reduction in safety. For example, significant unevenness on surfaces primarily intended for pedestrians can lead users to stumble. For this reason, at the design stage it is necessary to know what height differences (*hd*) will be generated as a function of the block thickness (*t*) and length (*L*), the crown (and consequently the equivalent slope s_e), the cross-section shape, the joint (j_d) and the roadway widths (*W*). At the same time, during an acceptance test or an on-site verification of the successful laying of stone blocks, it is possible to measure the height differences between adjacent elements and compare them with the design ones. Once again, the stretcher bond laying pattern was taken as a reference. In addition, the width of the stone block is not included in the considered parameters. For each analysed camber, the maximum height difference (*hd*) were figured out, firstly as a function of the block thickness ($hd(t)$), keeping fixed the equivalent slope, and then as a function of equivalent slope ($hd(s_e)$), keeping fixed the stone block thickness. Some examples, referred to the straight and Allard parabolic cambers, are shown in Fig. 12.

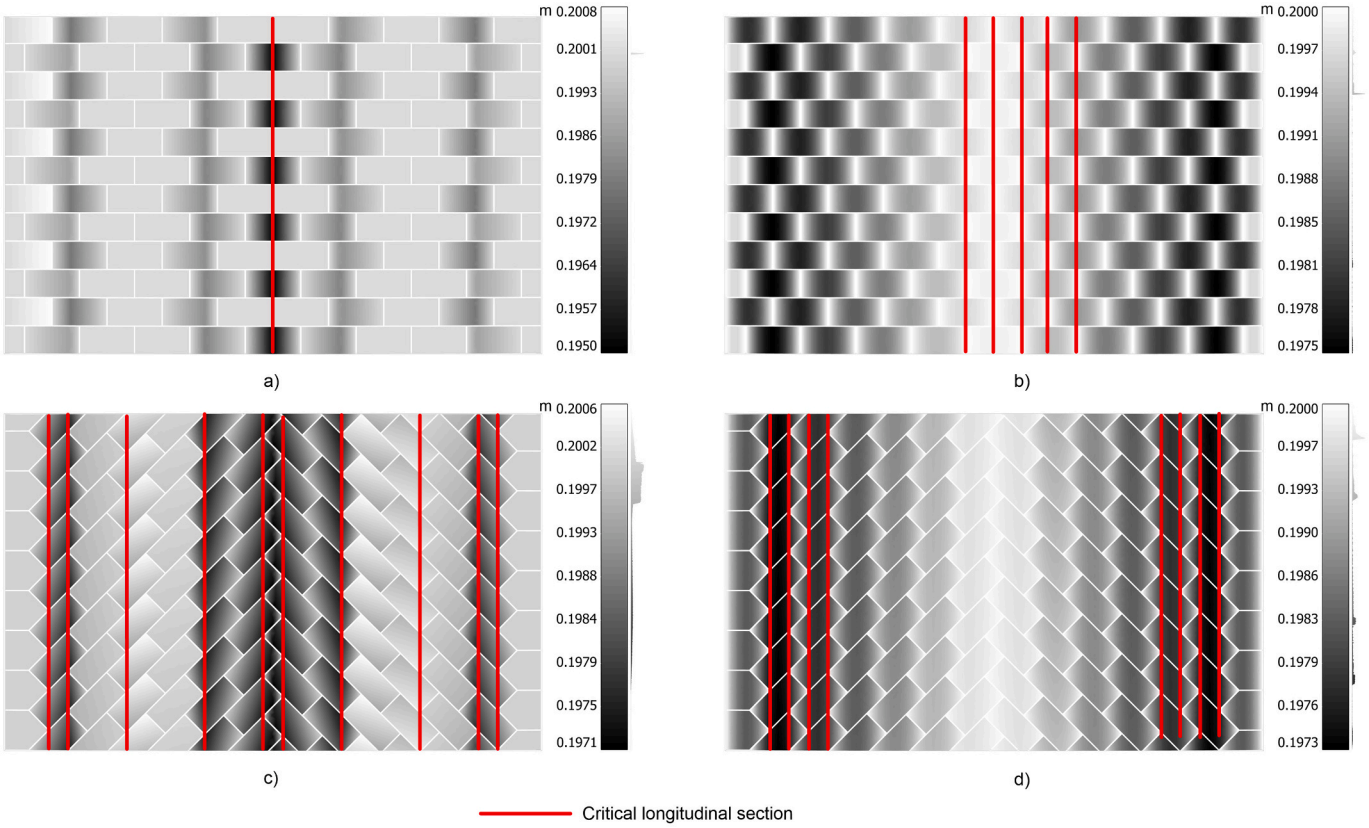

Fig. 11. False-colour images obtained from CloudCompare for a) stretcher bond laying pattern with multi-slope camber, b) stretcher bond laying pattern with Allard parabolic camber, c) converging stretcher bond laying pattern with multi-slope camber and d) converging stretcher bond laying pattern with Allard parabolic camber.

Table 1
Maximum height difference between adjacent elements.

Laying patterns	Camber							
	Straight		Multi-slope		Allard		Cubic	
	hd [mm]	Loc.	*hd* [mm]	Loc.	*hd* [mm]	Loc.	*hd* [mm]	Loc.
Stacked bond	0.00	–	0.00	–	0.00	–	0.00	–
Stretcher bond	5.47	C	4.86	C	2.00	C	2.34	L
Stretcher bond 45°	2.49	C	2.80	C	2.47	L	2.25	L
Converging stretcher bond	3.24	C	2.58	C	1.19	C	2.31	L
Herringbone 45°	3.68	C	2.70	C	1.25	C	2.26	L

Loc. = longitudinal critical section location; C = centre strip; L = lateral strip.

As can be seen, hd is constant for both cambers as t changes ($hd(t) = cost$), while the trends of hd as a function of s_e are well interpolated by straight lines passing through the origin. The greatest growth as a function of s_e (with $t = const$) was observed for the straight camber with double growth compared to the multi-slope camber, 4 times compared to the cubic parabolic camber, and 10 compared to the Allard camber, which is thus the section with the lowest growth. For all the analysed combinations, the maximum hd was found in the central part for the straight and the multi-slope cambers, in the lateral part for the cubic parabolic camber while it was approximatively constant along the whole section for the Allard camber.

The same analysis was conducted by varying the other parameters one at a time, i.e., block length (L), joint design width (j_d) and roadway width (W). An example of hd as a function of L ($hd(L)$) for the cubic parabolic camber is represented in Fig. 13a. As illustrated, $hd(L)$, by fixing s_e and t, can be interpolated with a power function $hd(L) = \gamma \times L^{\delta}$ in which γ and δ depend on s_e, t and the camber. The same trend was observed for $hd(W)$, while $hd(j_d)$ was constant.

A coefficient c_m (with $m = 4$ for slab length and $m = 5$ for roadway width) was introduced to obtain the trend of hd independently of the previously obtained vales (i.e., $hd(s_e)$), using the Eq. (9):

$$c_m = \frac{hd(m_v)}{hd(m_{v\_ref})} \tag{9}$$

in which m_v is the parameter value (L, j_d or W) and m_{v_ref} is the parameter reference value ($L = 80$ cm, $j_d = 20$ mm and $W = 8$ m). An example of $c_4(L)$ for the cubic parabolic camber is shown in Fig. 13b. As can be seen also $c_4(L)$ can be interpolated by a power function. By repeating these analyses for the different cross sections, it is possible to obtain the nomograms represented in Fig. 14, from which the maximum expected height difference (hd_{max}) can be calculated through Eq. (10):

$$hd_{max} = hd(s_e) \times c_4 \times c_5 \tag{10}$$

in which $hd(s_e)$ can be read from the left nomograms and $c_4$and c_5 from the right nomograms of Fig. 14.

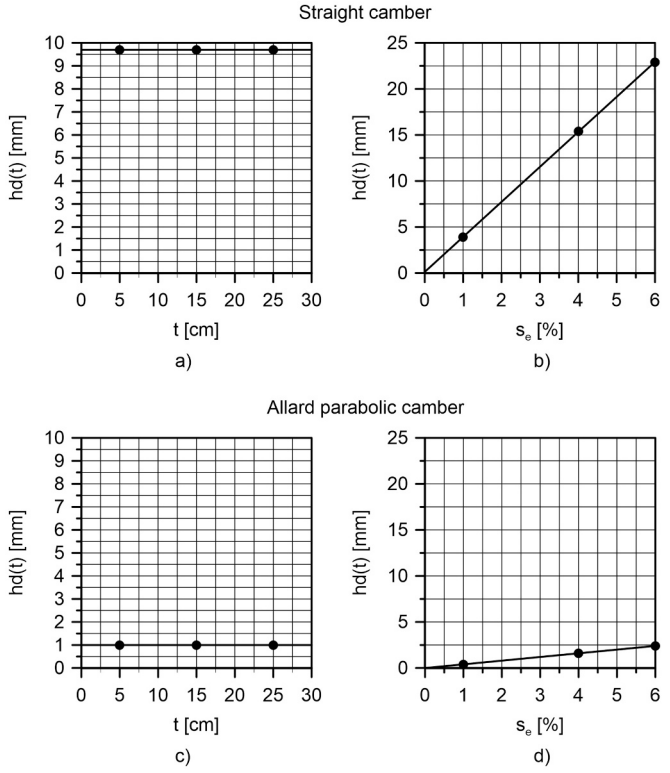

Fig. 12. a) *hd* vs *t* and b) *hd* vs s_e for straight camber and c) *hd* vs *t* and d) *hd* vs s_e for Allard parabolic camber and stretcher bond laying pattern.

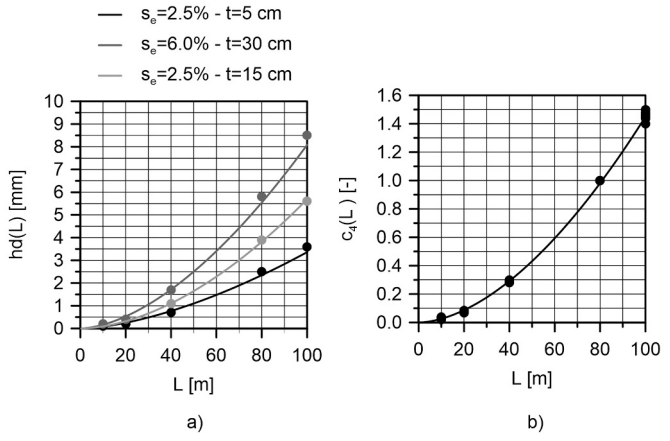

Fig. 13. a) $hd(L)$ vs L and b) $c_4(L)$ vs L for cubic parabolic camber and stretcher bond laying patter.

A practical example of using nomograms to determine the maximum expected height difference is given. A pavement made with stone blocks having a length of 50 cm and a thickness of 15 cm arranged in a stretcher bond laying pattern is considered. The joint design width is set to 10 mm. The cross section has a cubic parabolic shape with an equivalent slope equal to 3%. The roadway width is 7 m. It is necessary to refer to the Fig. 14c to solve this problem. From the first nomogram it is possible to determine:

$$hd(s_e) = hd(3) = 2.9\ mm,$$

$$c_4(L) = c_4(50) = 0.43$$

$$c_5(W) = c_5(7) = 1.15$$

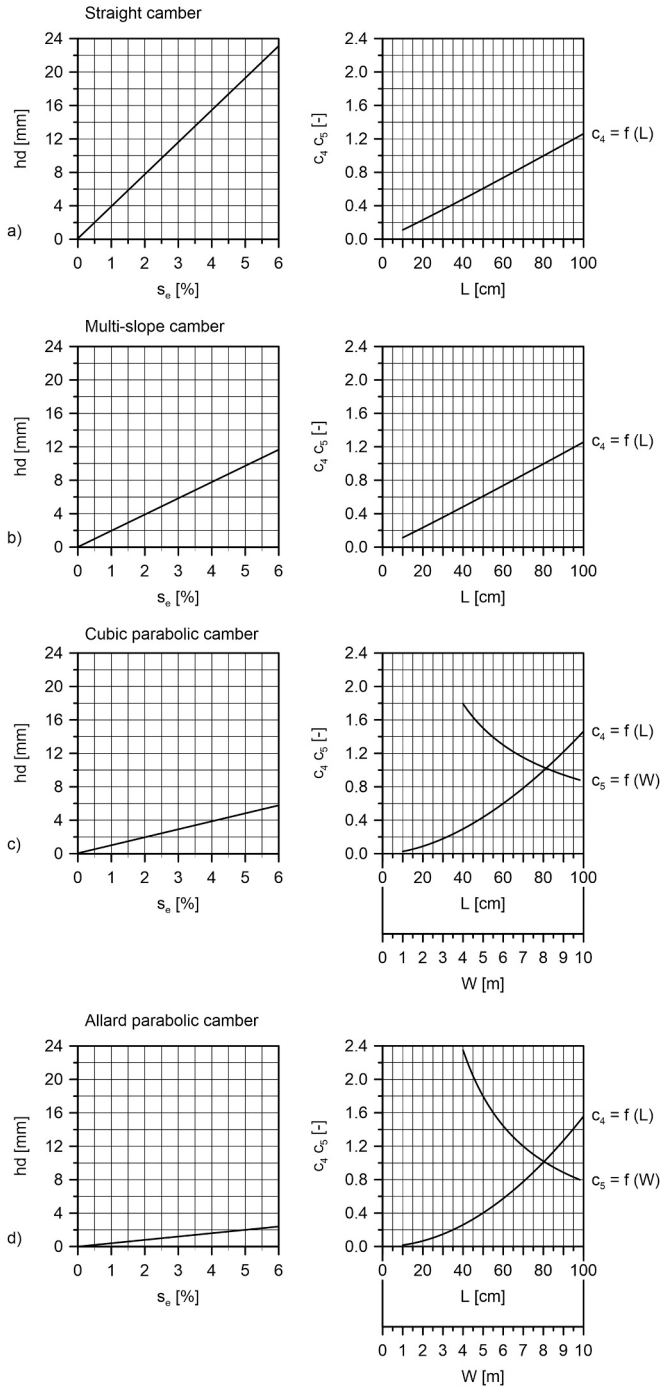

Fig. 14. Nomogram for determination of *hd* for stretcher bond laying pattern and a) straight, b) for multi-slope, c) cubic parabolic and d) second order (Allard) parabolic camber.

At this point, the maximum height difference of adjacent elements on the pavement surface (hd_{max}) can be calculated as

$$hd_{max} = hd(s_e) \times c_4 \times c_5 = 2.9 \times 0.43 \times 1.15 = 1.43\ mm.$$

6. Conclusions

Stone block pavements consist of discrete units placed close together and embedded in a bound or unbound bedding layer according to a given laying pattern. Design choices, in terms of laying pattern, cross-sectional shape and slope, as well as element shape and sizes, are not

exempt from causing inherent defects, which are essentially unrelated to supply and laying issues. The main inherent defects are the joint opening or closing and the height differences between adjacent elements. These defects, which cannot be eliminated but only limited by proper road design and construction, can compromise the aesthetic result and the mechanical resistance of the paving, as well as lead to both comfort and safety issues in both pedestrian-only areas, especially in presence of impaired users, and areas subject to vehicular traffic. The position and extent of such defects are benchmarks not available to date but essential in design, execution and validation phases along with disputes resolution between client and contractor.

Following analyses of a virtual 3D reference pavement layout (8 m wide roadway with an equivalent slope of 2.5%, consisting of 80 cm long, 40 cm wide and 20 cm high blocks spaced 20 mm apart), the locations and values of the main inherent defects were determined by varying the laying pattern and cross-section shape. Focusing on the stretcher bond laying pattern, one of the main solutions used for urban pavements, the authors developed nomograms that allow, through appropriate coefficients, to generalize these results to pavements with different cross-section slopes, stone block sizes (thickness and length), design joints and road widths. By analysing the reference pavement and reading the produced nomograms, it is possible to identify some behaviours associated with the main inherent defects:

- Considering the reference pavement layout, the greatest opening of the joint occurs for the straight camber for all the laying patterns. Whilst the joints are only opened across the section when the laying pattern uses blocks placed transversely to the carriageway axis, the joints are also closed when the laying pattern uses elements placed at 45° to the carriageway axis. The maximum joint opening is located close to the centreline in the case of linear cross sections (straight and multi-slope cambers), near the edges in the case of second-order parabolic camber, and it is approximately constant over the entire cross-section in the case of cubic parabolic camber. Considering only the stretcher bond laying pattern, the joint opening varies from a few millimetres to about three centimetres in extreme cases (high slopes, element sizes and design joint widths).
- As far as the height difference between adjacent elements is concerned, pavements with stacked bond or running bond laying pattern always show a zero value, due to their configuration. For the other laying patterns, the maximum height difference between adjacent elements is generally located close to the centreline except for the cubic parabolic camber for which is located near the edges. Considering again the only stretcher bond laying pattern, the maximum value varies from few tenths of millimetre to about three centimetres in extreme cases (high slopes, element sizes and design joint widths).

The obtained nomograms are ideal for evaluating the inherent defects of pavements made with cut stones, since the geometric variability between the different elements is limited, but they are still representative of pavements made with split elements. Thus, the use of such nomograms enables at the design stage to choose the best configuration not only according to the site category, but also in relation to the expected inherent defects. On the other hand, these nomograms allow verifying the correct execution of the pavement at the validation stage or in the case of disputes between client and contractor. A generalization to different types of laying patterns would be achievable by creating new graphs similar to those proposed. The implementation of a user-friendly software, which consider the nomograms as input data and the inherent defect as outputs, would be the final step in automating the process of block pavement design and the related quality control of the construction works, offering to designers and Public Administrations a new smart tool at their disposal.

CRediT authorship contribution statement

Erika Garilli: Writing – review & editing, Writing – original draft, Visualization, Methodology, Formal analysis. **Nazarena Bruno:** Writing – review & editing, Writing – original draft, Methodology, Conceptualization. **Federico Autelitano:** Writing – review & editing, Writing – original draft, Methodology, Conceptualization. **Felice Giuliani:** Writing – review & editing, Writing – original draft, Supervision, Methodology, Funding acquisition, Conceptualization.

Declaration of competing interest

The authors declare that they have no known competing financial interests or personal relationships that could have appeared to influence the work reported in this paper.

Data availability

Data will be made available on request.

Acknowledgements

Funder: Project funded under the National Recovery and Resilience Plan (NRRP), Mission 4 Component 2 Investment 1.5 - Call for tender No. 3277 of 30/12/2021 of Italian Ministry of University and Research funded by the European Union – NextGenerationEU.

Award Number: Project code ECS00000033, Concession Decree No. 1052 of 23/06/2022 adopted by the Italian Ministry of University and Research, CUP D93C22000460001, "Ecosystem for Sustainable Transition in Emilia-Romagna" (Ecosister). Spoke 4.

References

[1] E. Garilli, F. Giuliani, Stone pavement materials and construction methods in Europe and North America between the 19th and 20th century, Int. J. Architect. Heritage. 13 (2019) 742–768, https://doi.org/10.1080/15583058.2018.1470269.
[2] E.-S. Han, J. Gong, D. Cho, S.-K. Park, Experimental investigation on the application of ultra-rapid-hardening mortar for rigid small element pavement, Adv. Mater. Sci. Eng. 2019 (2019) 1–9, https://doi.org/10.1155/2019/2625437.
[3] E.-S. Han, J. Gong, H. Jeong, D. Cho, Development of bonded natural stone pavement using ultra-rapid-hardening mortar, Appl. Sci. (switzerland). 10 (2020) 1–12, https://doi.org/10.3390/app10103576.
[4] G. Tesoriere, Costruzione di strade ferrovie ed aeroporti, G. Denaro, 1963. OCLC 889400731.
[5] F. Autelitano, E. Garilli, F. Giuliani, Criteria for the selection and design of joints for street pavements in natural stone, Constr. Build. Mater. 259 (2020) 1–14, https://doi.org/10.1016/j.conbuildmat.2020.119722.
[6] E. Garilli, F. Autelitano, R. Roncella, F. Giuliani, The influence of laying patterns on the behaviour of historic stone pavements subjected to horizontal loads, Constr. Build. Mater. 258 (2020) 1–8, https://doi.org/10.1016/j.conbuildmat.2020.119657.
[7] E. Garilli, F. Autelitano, F. Freddi, F. Giuliani, Urban pedestrian stone pavements: measuring functional and safety requirements, Int. J. Pave. Eng. (2021) 1–12, https://doi.org/10.1080/10298436.2021.1975195.
[8] H. Murat Algin, Interlock mechanism of concrete block pavements, J. Transp. Eng. 133 (2007) 318–326, https://doi.org/10.1061/(ASCE)0733-947X(2007)133:5(318).
[9] E. Garilli, F. Autelitano, F. Freddi, F. Giuliani, Impact of pedestrian pavement design on the users' comfort level in an intermodal passenger terminal, Int. J. Pave. Res. Technol. (2023) 1–14, https://doi.org/10.1007/s42947-023-00366-z.
[10] P. Zoccali, G. Loprencipe, A. Galoni, Sampietrini stone pavements: distress analysis using pavement condition index method, Appl. Sci. 7 (2017) 1–22, https://doi.org/10.3390/app7070669.
[11] J. Knapton, I. Cook, Research and development in discrete element paving systems, Proc. Inst. Civ. Eng. Transp. 153 (2002) 13–23, https://doi.org/10.1680/tran.2002.153.1.13.
[12] B. Héritier, O. Dubost, Pierres naturelles: conception et réalisation de voiries et d'espaces publics, RGRA, Paris, 2019. ISBN 2913414524.
[13] F.J. Hugo, Camber and super-elevation, Civ. Eng. 1939 (1939) pp. 138–143. https://journals.co.za/doi/abs/10.10520/AJA10212019_18907 (accessed May 13, 2022).
[14] W.P. Judson, City Roads and Pavements Suited to Cities of Moderate Size, 2nd ed, The Engineering new Pub. Co, New York, 1902. LCCN 02019604.
[15] L. Stabilini, Lezioni di costruzioni stradali e ferroviarie, Cedam,Padova, 1939. LCCN 41040547.

[16] F. Balatroni, Vie e mezzi di trasporto: costruzioni stradali e ferroviarie, tecnica ed economia dei trasporti, Istituto Editoriale Cisalpino,Milano, 1949. LCCN 57033047.
[17] G. Maresca, Costruzioni stradali e ferroviarie, Roma 1946, BNI, 1945, p. 5616.
[18] W. Tartarini, Elementi di topografia e costruzioni stradali, Edizioni dell'ateneo, Roma, 1953 (LCCN a 53008595).
[19] D. Ruggeri, Studio e redazione dei progetti stradali e ferroviari, Casa editrice giuseppe principatp,Messina, 1939. OCLC 1277328258.
[20] B.J. Kerkhof, Strade in asfalto ed al catrame. Applicazioni stradali bituminose, Ulrico Hoepli,Milano, 1927. OCLC 860604540.
[21] A. Pasini, Costruzioni delle strade ordinarie e ferrate, Libreria editrice politecnica, Milano, 1923. OCLC 875787350.
[22] E. Garilli, N. Bruno, F. Autelitano, R. Roncella, F. Giuliani, Automatic detection of stone pavement's pattern based on UAV photogrammetry, Autom. Constr. 122 (2021) 1–14, https://doi.org/10.1016/j.autcon.2020.103477.
[23] Autodesk, AutoCAD 2024, 2023 https://www.autodesk.it/products/autocad/ (accessed October 5, 2022).
[24] L.J. Hopper, Landscape Architectural Graphic Standards, John Wiley & Sons, Inc, Hoboken, NJ, 2007. ISBN 9780471477556.
[25] H.-D. Hensel, Paving design: is rigid-fix external stone paving the way to go?, in, ASTM Spec. Tech. Publ. (2007) 27–39, https://doi.org/10.1520/JAI100843.
[26] P. Li, C.A. Fairfield, D. Fordyce, Design advice for rigid highway pavements constructed in natural stone, Proc. Inst. Civil Eng. Const. Mater. 165 (2012) 135–144, https://doi.org/10.1680/coma.11.00061.
[27] G. Blanco, Pavimentazioni in pietra, La Nuova Italia Scientifica, Roma, 1994. ISBN 8843002570.
[28] GitHub - CloudCompare, (n.d.). https://github.com/CloudCompare/CloudCompare (accessed October 5, 2022).
[29] N. Pham, W. Lin, H. Kim, Y. Cho, Evaluation methodology for laying pattern of interlocking concrete block pavements using a displacement-moment concept, J. Transp. Eng. 140 (2014) 1–7, https://doi.org/10.1061/(ASCE)TE.1943-5436.0000623.